mathematics

MDPI

Article

A Machine-Learning-Based Model for Buckling Analysis of Thermally Affected Covalently Functionalized Graphene/Epoxy Nanocomposite Beams

Farzad Ebrahimi * and Hosein Ezzati

Department of Mechanical Engineering, Faculty of Engineering, Imam Khomeini International University, Qazvin 34148-96818, Iran
* Correspondence: febrahimy@eng.ikiu.ac.ir

Abstract: In this paper, a machine-learning model is utilized to estimate the temperature-dependent moduli of neat, thermally reduced graphene and covalently functionalized graphene/epoxy nanocomposites. In addition, the governed mathematical expressions have been used to solve the buckling problem of beams fabricated from such nanocomposites in the presence of a thermal gradient. In order to do so, an energy-based method including the shear deformable beam hypothesis is used. The beam structure is rested on the Winkler–Pasternak substrate. The reported verifications demonstrate the impressive precision of the presented ML model, as well as the buckling response of the under-study structures. Finally, in the framework of some numerical case studies, the impact of several parameters on the buckling of nanocomposite beams is depicted. The results of this study delineate that temperature has a vital role in the determination of the critical buckling load that the nanocomposite structures can endure.

Keywords: machine learning; functionalized graphene nanocomposites; thermal buckling; shear deformable beam

MSC: 37M10

Citation: Ebrahimi, F.; Ezzati, H. A Machine-Learning-Based Model for Buckling Analysis of Thermally Affected Covalently Functionalized Graphene/Epoxy Nanocomposite Beams. *Mathematics* **2023**, *11*, 1496. https://doi.org/10.3390/math11061496

Academic Editors: Elena Benvenuti and Paolo Mercorelli

Received: 17 December 2022
Revised: 6 March 2023
Accepted: 14 March 2023
Published: 18 March 2023

1. Introduction

Researchers' capabilities for the study, development, and production of new and improved materials lie before efficient and, at the same time, accurate simulation methods. One of these novel ways is artificial intelligence which can take simulations to the next level. Over the past few years, machine learning (ML), which is a sub-category of artificial intelligence, has offered scientists and engineers new ways of interacting with data gathered from their studies. Scientists whose field of inquiry is the study of material properties, especially, can benefit from ML-based methods to predict a material's behavior based on a sufficient amount of data obtained from experimental studies. Furthermore, carbon-based nanocomposite (NC) materials have gained exceptional attention from the aerospace, mechanical, and other industries due to their beneficial mechanical properties. Research shows advantageous mechanical, thermal, and electrical characteristics in such carbonic nanocomposites. It is worth mentioning that these materials are often made by dispersing carbon-based reinforcements to a polymeric resin. Herein, a series of scientific objectives that have been met in the past is presented: The graphene oxide (GO) dispersion effect on the mechanical properties of graphene/epoxy composites was carried out by Tang et al. [1] using an experimental approach. Song et al. [2] investigated the high temperature effect on graphene oxide's structure and adsorption properties with flowing argon. The Raman stereoscopy method was implemented by Yadav and Cho [3] to enhance the mechanical and thermal properties of polyurethane nanocomposites by incorporating functionalized graphene nanoplates (f-GNP). In another experimental research performed

by Naebe et al. [4], graphene nanoplates (GNPs) were covalently functionalized in order to improve their bonding with the epoxy resin. Their investigation showed an increase in flexural strength and elastic modulus compared with GO due to the more consistent dispersion of functionalized graphene (FG). Furthermore, Chandrasekaran et al. [5] studied the addition of carbon-nanofiller-polymer-based epoxies and their effect on the fracture toughness and failure mechanism of the resultant NC. In another attempt, the impact of adding graphene platelets (GPLs) to a polymeric matrix on NC's fracture toughness was analyzed by Ahmadi-Moghadam and Taheri [6]. In addition, Sun et al. [7] developed empirical equations relating the mechanical properties of GO nanocomposites and their working temperature.

On top of the aforementioned experimental studies, numerous studies have been conducted about the static and dynamic responses of carbon-nanofiller-reinforced NCs with the use of a theoretical framework. For instance, Khoei and Khorrami [8] utilized a molecular dynamics analysis to assess the ultimate stress, Young modulus, and shear modulus of graphene oxide and compare the results with those of pure graphene. Moreover, Lin et al. [9] discussed the temperature-dependent Young's modulus of graphene oxide incorporated in polymer composites using molecular dynamics simulations. The natural frequencies of a multi-layer polymer NC reinforced with various GPL distributions were derived by Feng et al. [10]. In another study carried out by Kitipornchai et al. [11], GPLs were dispersed in the matrix with three different patterns, and, as the result, the free vibration and buckling of such functionally graded nanocomposites were assessed. Yas and Samadi [12] studied the buckling and free vibration response of beams fabricated from four types of carbon nanotube (CNT) distributions resting on an elastic foundation. By utilizing the principle of virtual work, Barati and Zenkour [13] were able to clarify the post-buckling behavior of graphene-platelet-reinforced nanocomposite (GPLRNC) beams with an imperfect porous geometry. Thereafter, Shen et al. [14] examined the nonlinear frequency response of graphene-reinforced nanocomposite (GRNC) beams with different types of distribution patterns along with the media's thickness. In another attempt, Yang et al. [15] succeeded in solving the thermal-bending problem of both circular and annular plates made of GPLRNCs with the use of the three-dimensional elasticity concept. By using the framework of the first-order shear deformation theory, Song et al. [16] succeeded in deriving both the bending and buckling responses of the GPLRNC plates. Concerned about the influence of porosities in the NC plates reinforced with GPLs, Yang et al. [17] surveyed the buckling and free vibration characteristics of such NC plates. In another endeavor, Yang et al. [18] studied the critical buckling response of GPLRNC plates by distributing the GPLs uniformly in each layer of multilayer plates. Moreover, the effects of a non-uniform magnetic field on the vibrational behavior of GO-reinforced nanocomposite (GORNC) beams were carried out by Ebrahimi et al. [19], utilizing a higher-order trigonometric beam model. Moayedi et al. [20] probed an analytical investigation on the thermal buckling answer of the GPLRNC cylindrical micro-panel. They used a higher-order shear deformable theory for obtaining the stress and strain response of the mentioned NC panels. In another research gathered by Mao and Zhang [21], piezoelectric plates reinforced with GPLs were subjected to both axial load and electric potential to study the buckling and post-buckling characteristics of such piezoelectric plates. Recently, machine-learning methods were implemented by Amini et al. [22] in order to derive the relationship between the elasticity moduli and the working temperature of various types of GORNCs. By doing so, they were able to obtain the critical buckling response of the GORNC beam with different GO weight fractions. Another paper regarding the buckling problem of GRNC beams developed by Yas and Rahimi [23] took into account the effects of the thermal environment and the existence of porosities in the NC. In addition, Shokrgozar et al. [24] deployed an analytical study on the dynamic and static response of a cylindrical micro-shell reinforced with GPLs covered with a viscoelastic foundation subjected to axial load. The dynamic behavior of GPL-reinforced porous plates with elastic boundary conditions was analyzed by Liu et al. [25]. Moreover, Qian et al. [26] probed the influence of the addition

of both functionalized and non-functionalized single-wall carbon nanotubes on the elastic modulus and tensile strength of incorporated glass/epoxy nanocomposites. With the use of an unconstrained higher-order theory, Eyvazian et al. [27] were able to determine the natural frequencies of cylindrical sandwich shells reinforced by GPLs. Lately, a thermal buckling analysis of GRNC beams with a negative thermal expansion coefficient using the Ritz method was carried out by Zhao et al. [28]. Furthermore, Jiang et al. [29] proposed a three-dimensional interface theory to develop a compatible multiscale model in order to examine the scaling law of the nanocomposites' effective moduli. Regarding the nanocomposite structures from ML-based approaches, TT Le [30] developed a model to predict the tensile strength of polymer CNTs using a database gathered from the literature. Moreover, Garg et al. [31] utilized a Gaussian process regression-based surrogate model as well as a finite element model to accurately evaluate the stiffness matrix of functionally graded nanoplates. In addition, a surrogate machine-learning model trained with MD models of functionalized CNT epoxy was developed by Rahman et al. [32] to precisely predict the CNT's pullout force.

To the authors' best knowledge, even though numerous studies have been conducted about the mechanical properties of NC materials and structures, nonetheless, there is no paper relating the mechanical characteristics of NC materials to its operational environment by utilizing artificial intelligence to further improve the efficiency and accuracy of the simulations. The main reason for this inquiry is the copious resources and amount of time that experimental studies require, along with the expensive hardware that conventional simulation methods need. This ensuing research is an attempt to link the mechanical properties of three types of NC materials with their working conditions. Motivated to make a bridge between theoretical relations and the experimental data, we utilized machine-learning methods to determine the relationship between an NC's Young's modulus and its temperature. Using these established mathematical relations derived for each NC type, we were able to easily access the Young's moduli of NC types in any desired temperature and ascertain the critical buckling load of three types of beams fabricated from neat epoxy, graphene-oxide-reinforced nanocomposite (GORNC), and functionalized graphene-reinforced nanocomposite (FGRNC) in a thermal environment. Here, we undertake the buckling analysis using a higher-order shear deformation theory. Moreover, the beam structure is rested on a medium with incorporated linear and shear springs. Moreover, the presented results regarding both moduli estimation and critical buckling load calculations are validated with previous research in order to show the precision of the presented model. Thereafter, a series of depicted reports are expressed to show the effects of different variants on the buckling behavior of NC beams.

2. Theory & Formulation

2.1. Problem Definition

Herein, the temperature dependency of GORNC, FGRNC, and neat epoxy will be derived using the experimental data gathered from the literature. Next, by utilizing the principle of virtual work, the buckling equations of beam-type elements will be obtained. In the end, an analytical solution will be presented to extract the critical buckling load of the simply-supported boundary conditions on each edge of the structure. Graphene reinforcements are distributed uniformly in the epoxy and the beam, as presented in Figure 1, embedded on a Winkler–Pasternak foundation. Moreover, the beam-type element used in the study has a length L, width b, and thickness of h.

2.2. Estimation of the Temperature-Dependent Young's Moduli

Although there are more simple ways to fit a curve to the experimental data, without the use of ML methods, the resultant expression would not be close enough to properly use the outcome for assessing the Young's modulus. For this reason, a machine-learning model based on regression was developed to extract an analytical expression for the estimation of the Young's moduli at any desired temperature. In order to do so, we derived the

experimental data reported by Naebe et al. [4]. The mentioned research has presented the variation of the moduli versus temperature raise for FG and GO nanocomposites. The reported weight fraction of the nanosized reinforcements is 0.1%. Figure 2 shows the Young's moduli of three types of material extracted experimentally by Naebe et al. [4].

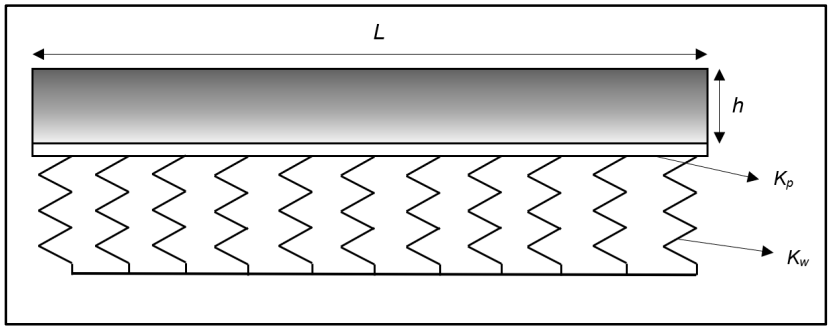

Figure 1. Configuration of a nanocomposite beam rested on an elastic substrate.

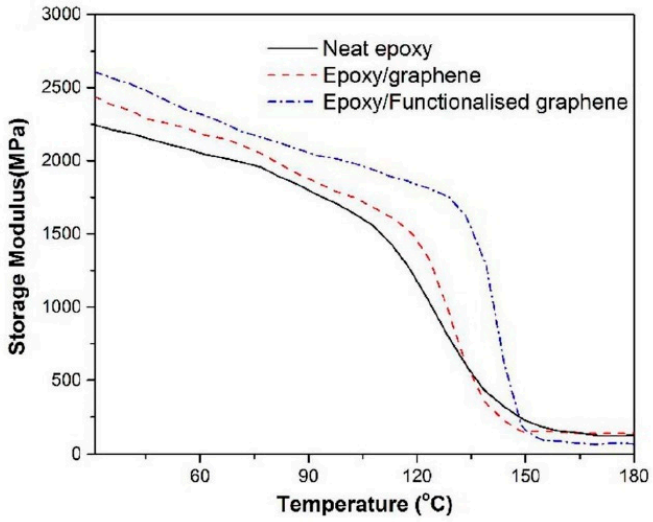

Figure 2. Young's moduli for neat epoxy and composite samples containing FG and GO [4].

After deriving a sufficient amount of data points from Figure 2, an ML-based regression procedure using multiple polynomial and sigmoid functions was initiated to obtain the best expression describing the dependency of Young's moduli on temperature. At the first stage of development, we used some polynomial and sigmoid functions in order to fit a curve to the experimental data. Afterwards, ML is deployed to reach appropriate estimation coefficients, as well as the proper number of terms for maximum accuracy. The model uses the standard deviation and the mean of the data for its initial guesses; after 50,000 tries, it presented the optimum value for each coefficient and the number of terms. The expression is as follows:

$$\begin{aligned} E = {} & \alpha_1 T + \alpha_2 T^2 + \alpha_3 T^3 + \alpha_4 \left(\frac{1}{1+\exp(-T+105)} \right) \\ & + \alpha_5 \left(\frac{1}{1+\exp(-T+115)} \right) + \alpha_6 \left(\frac{1}{1+\exp(-T+122)} \right) \\ & + \alpha_7 \left(\frac{1}{1+\exp(-T+125)} \right) + \alpha_8 \left(\frac{1}{1+\exp(-T+130)} \right) \\ & + \alpha_9 \left(\frac{1}{1+\exp(-T+135)} \right) + \alpha_{10} \left(\frac{1}{1+\exp(-T+140)} \right) \\ & + \alpha_{11} \left(\frac{1}{1+\exp(-T+145)} \right) + C \end{aligned} \quad (1)$$

where E is the Young's modulus, α_i are the estimation coefficients reported in Table 1 for each material type, and T is the desired temperature. Moreover, the term C indicates the

initial value of each of the types. For Equation (1), there is the assumption that there are no outliers in the reported experimental data, and that the temperature below and above the values reported are in continuous form. Of the 300+ points extracted from the experimental data, 77% was used to train the model, whilst the rest of the data was used to validate the outcome of this methodology. For an evaluation of the results, the root mean relative error (*MRE*) and R-squared (R^2) were implemented. Using the *MRE*, we found how close the regression line is to the experimental data, and it can be calculated using the following formula [33]:

$$MRE = \frac{\sum_{i=1}^{n}\left(\frac{\left|y_i - \bar{y_i}\right|}{\bar{y_i}}\right)}{n} \quad (2)$$

where n is the number of data points, and y_i and $\bar{y}_i$ are the experimental and the predicted data, respectively. An algorithm can be authenticated with these two methods (i.e., *MRE* and R^2) when the value of R^2 is very close to the perfect state of 1. In addition to validating the proposed algorithm, the value of *MRE* should be intensely less that the values of the data points. As shown in Table 2, the validity of the presented algorithm is confirmed by the values of both *MRE* and R^2.

Table 1. The estimation coefficients of different material types.

Neat epoxy (C = 2121.54893)					
α_1	α_2	α_3	α_4	α_5	α_6
7.80627389	$-1.81533262 \times 10^{-1}$	$5.99054633 \times 10^{-4}$	$-9.41097233 \times 10^{1}$	$-1.87784478 \times 10^{2}$	$-1.82985862 \times 10^{2}$
α_7	α_8	α_9	α_{10}	α_{11}	
$-8.19707494 \times 10^{1}$	$-1.86225844 \times 10^{2}$	$-1.30992530 \times 10^{2}$	$-6.71379619 \times 10^{1}$	$-8.64014610 \times 10^{1}$	
Epoxy/Graphene (C = 2394.51308)					
α_1	α_2	α_3	α_4	α_5	α_6
4.33776820	$-1.66278050 \times 10^{-1}$	$6.11193348 \times 10^{-4}$	$-2.42975958 \times 10^{1}$	$-7.63626419 \times 10^{1}$	$-1.33970188 \times 10^{2}$
α_7	α_8	α_9	α_{10}	α_{11}	
$-2.37603975 \times 10^{2}$	$-3.43333229 \times 10^{2}$	$-2.32259096 \times 10^{2}$	$-1.12062166 \times 10^{2}$	$-3.60855758 \times 10^{1}$	
Epoxy/Functionalized graphene (C = 2968.22288)					
α_1	α_2	α_3	α_4	α_5	α_6
$-1.22978891 \times 10^{1}$	$2.27421386 \times 10^{-2}$	$1.09216658 \times 10^{-5}$	1.61387358×10^{1}	$-1.34988115 \times 10^{1}$	$-1.25826021 \times 10^{1}$
α_7	α_8	α_9	α_{10}	α_{11}	
$-1.15675331 \times 10^{1}$	$-9.50302118 \times 10^{1}$	$-2.01753507 \times 10^{2}$	$-5.76713858 \times 10^{2}$	$-6.21085483 \times 10^{2}$	

Table 2. R^2 and MRE values for training and test datasets of the materials.

Material	**R^2**		**MRE**	
	Training Dataset	**Test Dataset**	**Training Dataset**	**Test Dataset**
Neat epoxy	0.9997	0.9994	0.0006	0.0006
Epoxy/Graphene	0.9997	0.9996	0.0006	0.0005
Epoxy/Functionalized graphene	0.9992	0.9987	0.0007	0.0006

Figure 3 show the error distributions for the Young's moduli of the three types of materials under study. As it is demonstrated in this plot, the errors can be negligible when compared to the actual value of the Young's moduli. Furthermore, Table 3 shows the proximity of the moduli calculated by the regressed model and those reported in the literature. Therefore, the proposed expression can accurately estimate the Young's moduli of nanocomposites at any desired temperature.

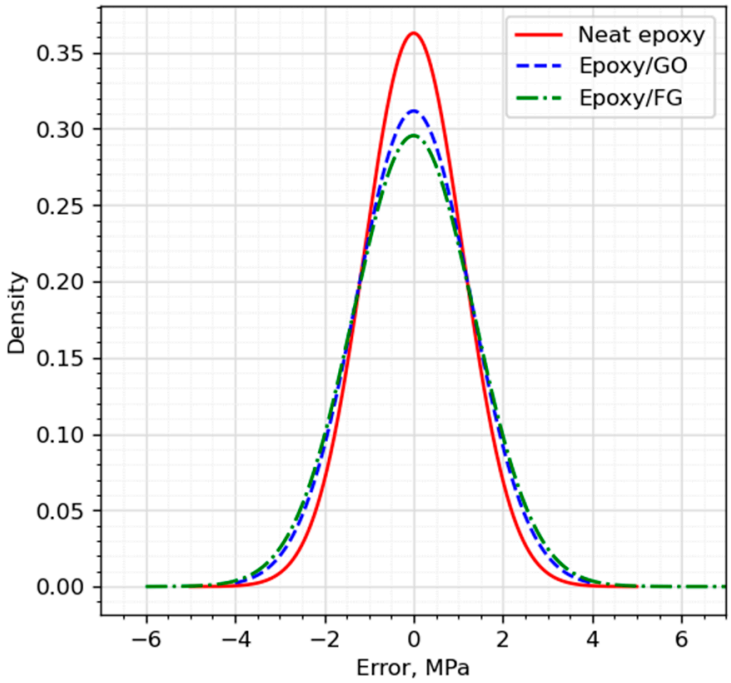

Figure 3. Error distributions for Young's moduli of neat epoxy, epoxy/GO, and epoxy/FG.

Table 3. Comparison of the estimated and experimental values of the Young's moduli for the studied material types.

	Neat Epoxy		**Epoxy/Graphene**		**Epoxy/Functionalized Graphene**	
Temp	**Actual [4]**	**Fitted**	**Actual [4]**	**Fitted**	**Actual [4]**	**Fitted**
40	2180.7	2179.3	2337.5	2341.5	2514.1	2513.4
50	2131.5	2129.0	2273.8	2274.4	2410.7	2411.5
60	2066.2	2067.3	2186.8	2188.1	2313.0	2314.6
70	1980.0	1977.9	2089.1	2090.4	2217.3	2222.5
80	1902.4	1886.5	1986.6	1986.5	2135.7	2135.7
90	1784.8	1785.8	1874.5	1877.6	2054.4	2053.6
100	1678.6	1683.4	1774.4	1776.5	1985.2	1976.8
110	1485.6	1483.7	1647.3	1648.5	1918.8	1921.1
120	1185.5	1181.7	1457.9	1459.0	1840.1	1839.8
130	741.7	740.3	848.0	847.2	1707.8	1707.5
140	402.4	407.0	317.4	317.3	1121.0	1112.7
150	214.3	213.6	164.8	170.9	159.4	160.1
160	156.7	160.0	150.2	139.3	97.7	111.4
170	124.1	126.4	135.5	133.3	65.9	72.4
180	120.4	120.7	139.1	146.4	54.8	39.0

As shown in Figure 4 and Tables 1–3, the results of our modeling are in excellent agreement with the experimental results reported by Naebe et al. [4]. It is obvious that the model presented is capable of estimating the elasticity moduli for the mentioned nanocomposites with high precision. Therefore, it is reasonable to use the expression obtained from this modeling instead of the experimental data in order to accelerate the analysis of the mechanical behaviors of such nanocomposites in thermal environments for future studies.

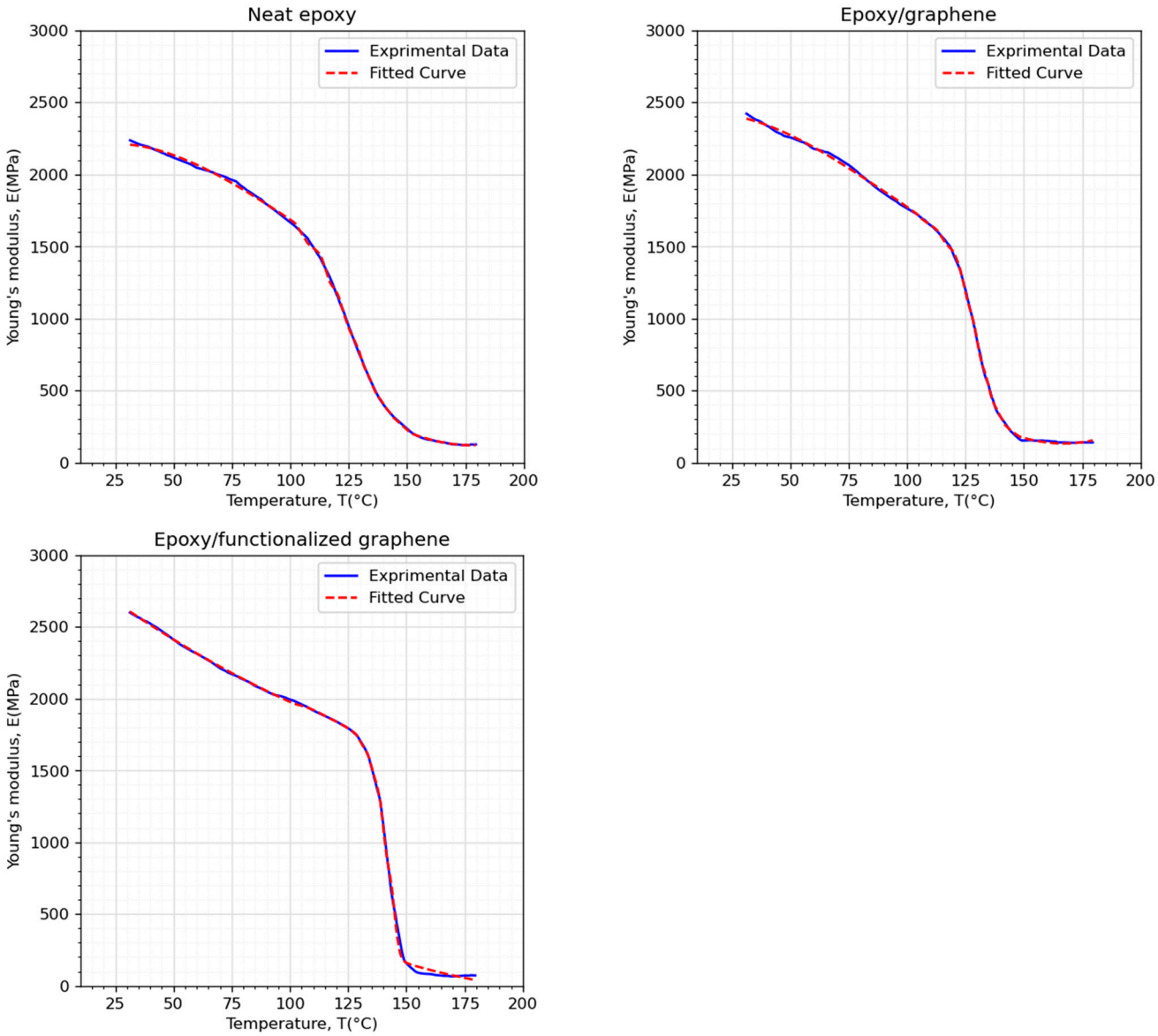

Figure 4. Comparison of the experimental data for the Young's moduli of neat epoxy, epoxy/G, and epoxy/FG reported by Naebe et al. [4] with the fitted curves.

2.3. The Governing Equation for Thermally Affected Buckling Problem

In order to solve the buckling problem of a beam, using Hamilton's principle is a suitable method. For the sake of brevity, the derivation process will not be expanded in this paper and the thorough procedure can be found in the literature. In this section, the governing equations needed to solve the buckling problem in the presence of the temperature gradient of the refined shear deformable beam will be presented. These partial differential equations have been obtained on the basis of the principle of virtual work. The equations of motion have been developed in the framework of a Hamiltonian approach. Afterward, the elastic stress–strain relations of the nanocomposite materials were reviewed in order to extract the fundamental elastic equations of such solids. Finally, the governing equations of motion can be expressed as [34,35]:

$$A\frac{\partial^2 u}{\partial x^2} - B\frac{\partial^3 w_b}{\partial x^3} - B_s\frac{\partial^3 w_s}{\partial x^3} = 0 \tag{3}$$

$$B\frac{\partial^3 u}{\partial x^3} - D\frac{\partial^4 w_b}{\partial x^4} - D_s\frac{\partial^4 w_s}{\partial x^4} + k_w(w_b + w_s) - \left(k_p - N^T\right)\frac{\partial^2(w_b + w_s)}{\partial x^2} = 0 \quad (4)$$

$$B_s\frac{\partial^3 u}{\partial x^3} - D_s\frac{\partial^4 w_b}{\partial x^4} - H_s\frac{\partial^4 w_s}{\partial x^4} + A_s\frac{\partial^2 w_s}{\partial x^2} + k_w(w_b + w_s) - \left(k_p - N^T\right)\frac{\partial^2(w_b + w_s)}{\partial x^2} = 0 \quad (5)$$

where u, w_b, and w_s are the longitudinal displacement, bending, and shear deflection, respectively. Moreover, the terms A, B, B_s, D, D_s, H_s, and A_s are the cross-sectional rigidities that can be defined as mentioned in Ebrahimi and Barati [34], and Ebrahimi and Dabbagh [35]. Moreover, k_w and k_p denote the Winkler–Pasternak elastic coefficients of the medium which are under the beam-type element. Finally, N^T stands for the thermal loading produced from the existence of a uniform temperature gradient. In more detail, an arbitrary point of the nanocomposite beam is assumed to be subjected to a uniform temperature raise (i.e., $\Delta T = T - T_0$; where T is the local and T_0 is the initial temperature). Any complementary information about the derivation of the above expressions, as well as the mentioned variants, along with their mathematical representation, can be found by referring to [34,35].

3. Analytical Solution

There are numerous methods for solving mechanical problems analytically. Here, we used Navier's solution to extract the critical buckling load of the beam under the conditions previously stated. The corresponding boundary conditions for a simply-supported beam can be illustrated as:

$$w_b = w_s = 0, \ \frac{\partial^2 w_b}{\partial x^2} = \frac{\partial^2 w_s}{\partial x^2} = 0 \text{ at } x = 0, L \quad (6)$$

Here, we are assuming that the beam's sides cannot move; moreover, they are presumed to be immovable ends. Now, the following solution functions can be applied to the displacement fields to satisfy the above-mentioned boundary condition:

$$u(x) = \sum_{n=1}^{\infty} U_n cos\left(\frac{n\pi x}{L}\right) \quad (7)$$

$$w_b(x) = \sum_{n=1}^{\infty} W_{bn} sin\left(\frac{n\pi x}{L}\right) \quad (8)$$

$$w_s(x) = \sum_{n=1}^{\infty} W_{sn} sin\left(\frac{n\pi x}{L}\right) \quad (9)$$

where, U_n, W_{bn}, and W_{sn} are referred to as unknown Fourier coefficients. By inserting the Equations (7)–(9) in Equations (3)–(5), the following relation can be obtained:

$$[K]_{3\times 3}\begin{Bmatrix} U_n \\ W_{bn} \\ W_{sn} \end{Bmatrix} = \{0\} \quad (10)$$

in which $[K]$ is the stiffness matrix and $\begin{Bmatrix} U_n \\ W_{bn} \\ W_{sn} \end{Bmatrix}$ is the displacement vector. To solve for the critical buckling value, the determinant of the stiffness matrix will be set to zero. Once this mathematical operation is performed, the critical buckling load of the simply-supported beam can be derived.

4. Results and Discussion

In this part, a sequence of illustrations will be represented to look into the influence of various terms on the buckling behaviors of beam structures made from neat epoxy,

GORNC, and FGRNC. First off, we validate the presented methodology by comparing the mechanical responses obtained from our modeling with those reported in the literature. To do so, the results from this study are set side by side with those reported by Yas and Samadi [12] in Table 4. Based on this comparison, it is evident that the method presented in this paper to predict the buckling characteristics of NC beams is valid.

Table 4. Comparison of the dimensionless critical buckling load of (C-C) CNTRNC beams (L/h = 15).

Volume Fraction of CNT,	**Reference**	
V^*_{CNT}	**Yas and Samadi [12]**	**Present**
0.12	0.213958	0.213564
0.17	0.344251	0.342843
0.28	0.455602	0.460245

Now, the effects of various types of reinforcements on the fundamental buckling mode (i.e., first mode) of the NC beams will be investigated. In order to better understand the numerical studies, first, the dimensionless form of the critical buckling load and foundation coefficients are presented as [22]:

$$N_{cr} = N^b \frac{L^2}{E_{FG} I},\ K_w = k_w \frac{L^4}{E_{FG} I},\ K_p = k_p \frac{L^2}{E_{FG} I},\ I = \frac{bh^3}{12} \tag{11}$$

in which N_{cr} is the dimensionless buckling load, and I denotes the second moment of area. Figure 5 illustrates the change in the buckling loads of the NCs versus the temperature raise. It is worth mentioning that the weight fractions of both GO and FG dispersed in the matrix are considered to be 1%. It can be realized that with the increase in temperature, the buckling load of the nanocomposite beam decreases. This phenomenon occurs because of the softening impact that the temperature gradient has on the stiffness of the nanocomposite system. Since the stiffness of a material has a direct relation to its buckling load, the buckling load fluctuates with the increment of temperature. Another case revealed by Figure 5 is that, near 30 degrees (i.e., room temperature), the buckling load of the FG-reinforced nanocomposite beam is more compared to the GO-reinforced and neat epoxy composites. However, the FG-reinforced beam has the most drastic drop in buckling load as the temperature increases. After that, the second most drastic decrease belongs to the beam made from the GO-reinforced nanocomposite, and the beam fabricated from pure epoxy has the lowest buckling load reduction. The main reason for the buckling load's fluctuation with the temperature raise is the negative value of the coefficient of thermal expansion (CTE) for graphene.

As the graphene mixes in the matrix, which has a positive value of CTE, it has a reduction effect on the CTE of the whole mixture. Hence, the lower weight fraction of graphene in the composite results in a higher CTE compared to the high concentration of graphene reinforcement. Therefore, when the composite system is set to work in environments with high temperatures, it is preferable to use lesser-weight fractions of FG or GO.

Figure 6 is depicted with the goal of studying the impact of both the slenderness ratio of the beam and the temperature gradients on the stability behaviors of the FGRNC beam. Based on this figure, with the rise of the slenderness ratio of the beam, the dimensionless buckling load declines non-linearly. This behavior can be explained by the more flexible geometry of the beam types that comes along as the slenderness ratio rises. The ensuing stiffness, which has an inverse relationship with flexibility, decreases gradually. Hence, as discussed earlier, the value of the buckling load abates with the reduction of stiffness. However, this downturn can be much harsher as the temperature gradient increments. Moreover, if the slenderness ratio of the nanocomposite beam reaches its critical value, the buckling load can even go as low as zero (i.e., the neutral stable state).

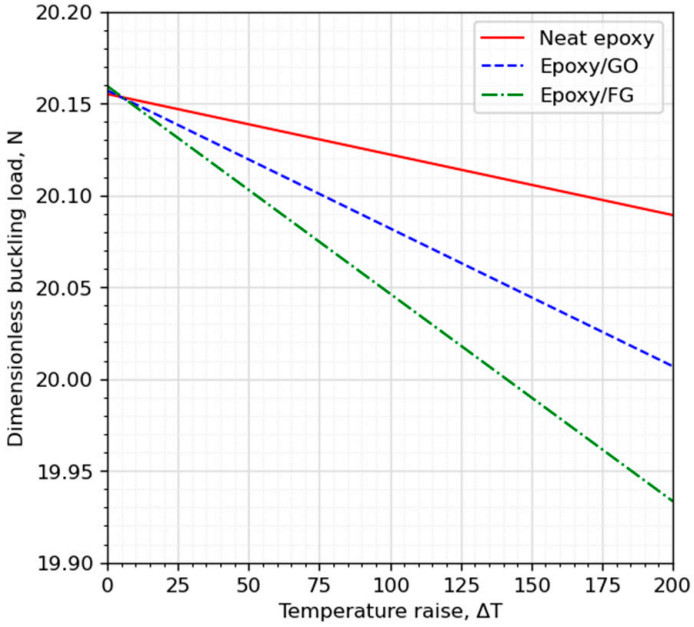

Figure 5. Variation of the first dimensionless buckling load of NC beams versus the temperature raise ($W_{GO/FG}$ = 1%, L/h = 20, Kw = 100, Kp = 10).

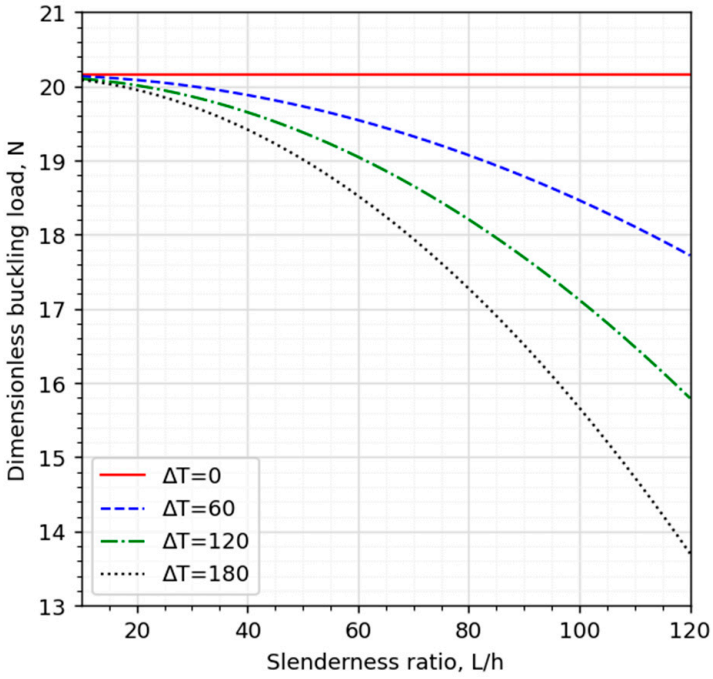

Figure 6. Variation of the first dimensionless buckling load of NC beams versus slenderness ratio (W_{FG} = 1%, Kw = 100, Kp = 10).

Figure 7 describes the change in the dimensionless buckling load of the NC beam against the Winkler coefficient for a number of temperature gradients. According to this plot, the buckling load is heavily dependent on the value of the Winkler coefficient. It is obvious that the stability limit of the beam can be enlarged by resting the structure on an elastic substrate. The amplifying effect of the Winkler coefficient on the continuous system's equivalent stiffness can explain this trend. In addition, it is shown by this diagram that the rise in temperature can result in the reduction of the dimensionless buckling load.

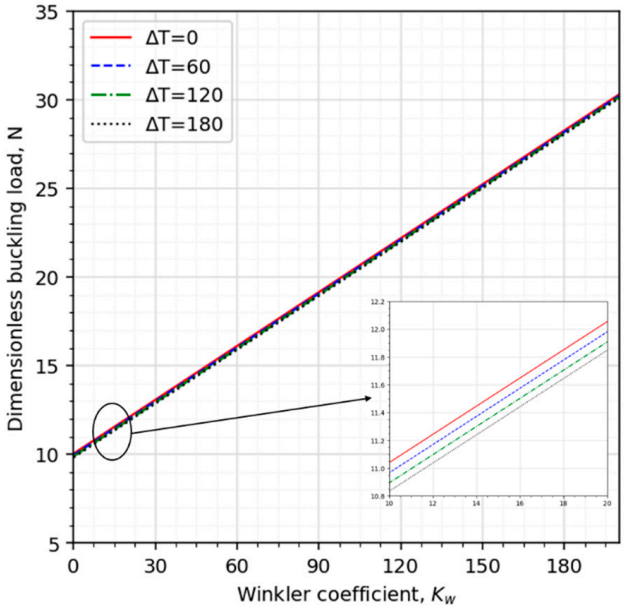

Figure 7. Variation of the first dimensionless buckling load of NC beams versus the Winkler coefficient (W_{FG} = 1%, L/h = 20, Kp = 10).

In another examination illustrated in Figure 8, the impact of both the Pasternak coefficient and temperature raise on the critical buckling load of the nanocomposite beam was studied. It is clear that by assigning higher values to the Pasternak coefficient, the structure gains more power and can tolerate more static loads. The reasoning for this behavior was unraveled in the previous paragraph; hence, it will not be explained here again. As it is the same as the former inquiry, it is comprehensible that, when the nanocomposite beam is subjected to thermal loading, by aggrandizing the thermal gradient, the buckling load will decrease gradually. It is interesting to point out the impact of both foundation parameters and compare them to one another. The critical buckling load can be incremented by a factor of two, by increasing the Winkler coefficient from zero to 100. However, the same effect can be generated by altering the Pasternak coefficient from zero to 10. Therefore, the Pasternak coefficient has more influence on the matter than the Winkler coefficient.

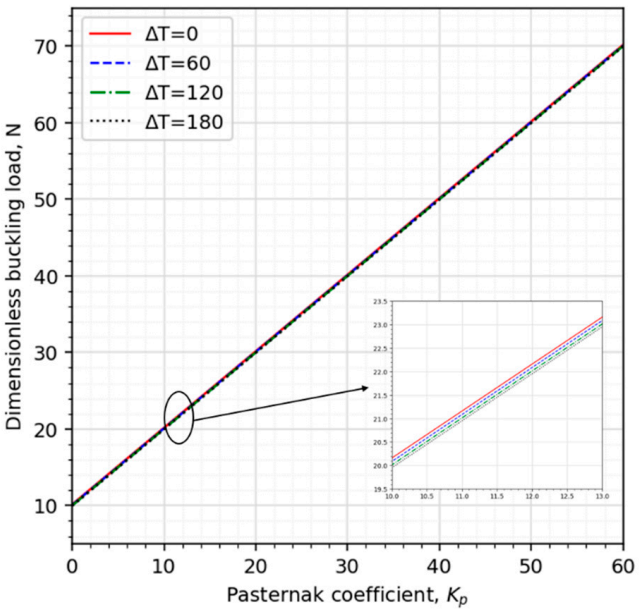

Figure 8. Variation of the first dimensionless buckling load of NC beams versus the Pasternak coefficient (W_{FG} = 1%, L/h = 20, Kw = 100).

5. Conclusions

This study was motivated to present a continuous analytical function to accurately estimate the Young's moduli of FG-reinforced nanocomposites at any desired temperature. Regression in the form of an ML model was utilized to extract the appropriate estimation coefficients for the proposed polynomial and sigmoid functions. Based on this study, it is recommended that further investigations for these materials take advantage of this mathematical expression for faster and more accurate results. The presented model can be used by finite element software for scientific and engineering endeavors. The ensuing developed model was put to work to determine the thermo-elastic stability of nanocomposite beams using Hamilton's principle. Afterwards, the Navier's solution was implemented to solve the governing PDEs and derive the stiffness and mass matrices. By setting determinant of the stiffness matrix, the critical buckling load was derived. Then, a comparison between the critical buckling load of FGRNCs and GORNCs was conducted. It was also realized that the beams become more flexible when exposed to higher values of a temperature raise. In conclusion, the FGRNC was shown to have a greater elastic modulus compared to GORNC. However, the temperature raise had a more drastic effect on the FGNRC because of the negative value of CTE. Hence, this research recommends implementing lower weight fractions of graphene reinforcements when the structure is subjected to immense thermal loading.

Author Contributions: Software, H.E.; Validation, H.E.; Formal analysis, H.E.; Investigation, F.E.; Resources, F.E.; Data curation, F.E.; Writing—original draft, F.E.; Project administration, F.E. All authors have read and agreed to the published version of the manuscript.

Funding: This research received no external funding.

Data Availability Statement: The data presented in this study are available in [4].

Conflicts of Interest: The authors declare no conflict of interest during this study.

References

1. Tang, L.-C.; Wan, Y.-J.; Yan, D.; Pei, Y.-B.; Zhao, L.; Li, Y.-B.; Wu, L.-B.; Jiang, J.-X.; Lai, G.-Q. The effect of graphene dispersion on the mechanical properties of graphene/epoxy composites. *Carbon* **2013**, *60*, 16–27.
2. Song, L.; Khoerunnisa, F.; Gao, W.; Dou, W.; Hayashi, T.; Kaneko, K.; Endo, M.; Ajayan, P.M. Effect of high-temperature thermal treatment on the structure and adsorption properties of reduced graphene oxide. *Carbon* **2013**, *52*, 608–612.
3. Yadav, S.K.; Cho, J.W. Functionalized graphene nanoplatelets for enhanced mechanical and thermal properties of polyurethane nanocomposites. *Appl. Surf. Sci.* **2013**, *266*, 360–367.
4. Naebe, M.; Wang, J.; Amini, A.; Khayyam, H.; Hameed, N.; Li, L.H.; Chen, Y.; Fox, B. Mechanical property and structure of covalent functionalised graphene/epoxy nanocomposites. *Sci. Rep.* **2014**, *4*, 4375.
5. Chandrasekaran, S.; Sato, N.; Tölle, F.; Mülhaupt, R.; Fiedler, B.; Schulte, K. Fracture toughness and failure mechanism of graphene based epoxy composites. *Compos. Sci. Technol.* **2014**, *97*, 90–99.
6. Ahmadi-Moghadam, B.; Taheri, F. Influence of graphene nanoplatelets on modes I, II and III interlaminar fracture toughness of fiber-reinforced polymer composites. *Eng. Fract. Mech.* **2015**, *143*, 97–107.
7. Sun, Z.; Li, Y.-Q.; Huang, P.; Cao, H.-J.; Zeng, W.; Li, J.; Li, F.; Sun, B.-G.; Shi, H.-Q.; Zhou, Z.-l. Temperature-dependent mechanical properties of polyetherimide composites reinforced by graphene oxide-coated short carbon fibers. *Compos. Struct.* **2021**, *270*, 114075.
8. Khoei, A.; Khorrami, M. Mechanical properties of graphene oxide: A molecular dynamics study. *Fuller. Nanotub. Carbon Nanostruct.* **2016**, *24*, 594–603. [CrossRef]
9. Lin, F.; Xiang, Y.; Shen, H.-S. Temperature dependent mechanical properties of graphene reinforced polymer nanocomposites–a molecular dynamics simulation. *Compos. Part B Eng.* **2017**, *111*, 261–269.
10. Feng, C.; Kitipornchai, S.; Yang, J. Nonlinear free vibration of functionally graded polymer composite beams reinforced with graphene nanoplatelets (GPLs). *Eng. Struct.* **2017**, *140*, 110–119.
11. Kitipornchai, S.; Chen, D.; Yang, J. Free vibration and elastic buckling of functionally graded porous beams reinforced by graphene platelets. *Mater. Des.* **2017**, *116*, 656–665. [CrossRef]
12. Yas, M.; Samadi, N. Free vibrations and buckling analysis of carbon nanotube-reinforced composite Timoshenko beams on elastic foundation. *Int. J. Press. Vessel. Pip.* **2012**, *98*, 119–128. [CrossRef]
13. Barati, M.R.; Zenkour, A.M. Post-buckling analysis of refined shear deformable graphene platelet reinforced beams with porosities and geometrical imperfection. *Compos. Struct.* **2017**, *181*, 194–202. [CrossRef]
14. Shen, H.-S.; Lin, F.; Xiang, Y. Nonlinear vibration of functionally graded graphene-reinforced composite laminated beams resting on elastic foundations in thermal environments. *Nonlinear Dyn.* **2017**, *90*, 899–914. [CrossRef]

15. Yang, B.; Kitipornchai, S.; Yang, Y.-F.; Yang, J. 3D thermo-mechanical bending solution of functionally graded graphene reinforced circular and annular plates. *Appl. Math. Model.* **2017**, *49*, 69–86.
16. Song, M.; Yang, J.; Kitipornchai, S. Bending and buckling analyses of functionally graded polymer composite plates reinforced with graphene nanoplatelets. *Compos. Part B Eng.* **2018**, *134*, 106–113. [CrossRef]
17. Yang, J.; Chen, D.; Kitipornchai, S. Buckling and free vibration analyses of functionally graded graphene reinforced porous nanocomposite plates based on Chebyshev-Ritz method. *Compos. Struct.* **2018**, *193*, 281–294.
18. Yang, J.; Dong, J.; Kitipornchai, S. Unilateral and bilateral buckling of functionally graded corrugated thin plates reinforced with graphene nanoplatelets. *Compos. Struct.* **2019**, *209*, 789–801. [CrossRef]
19. Ebrahimi, F.; Dabbagh, A.; Civalek, Ö. Vibration analysis of magnetically affected graphene oxide-reinforced nanocomposite beams. *J. Vib. Control* **2019**, *25*, 2837–2849. [CrossRef]
20. Moayedi, H.; Aliakbarlou, H.; Jebeli, M.; Noormohammadiarani, O.; Habibi, M.; Safarpour, H.; Foong, L. Thermal buckling responses of a graphene reinforced composite micropanel structure. *Int. J. Appl. Mech.* **2020**, *12*, 2050010. [CrossRef]
21. Mao, J.-J.; Zhang, W. Buckling and post-buckling analyses of functionally graded graphene reinforced piezoelectric plate subjected to electric potential and axial forces. *Compos. Struct.* **2019**, *216*, 392–405.
22. Amani, M.A.; Ebrahimi, F.; Dabbagh, A.; Rastgoo, A.; Nasiri, M.M. A machine learning-based model for the estimation of the temperature-dependent moduli of graphene oxide reinforced nanocomposites and its application in a thermally affected buckling analysis. *Eng. Comput.* **2021**, *37*, 2245–2255.
23. Yas, M.-H.; Rahimi, S. Thermal buckling analysis of porous functionally graded nanocomposite beams reinforced by graphene platelets using Generalized differential quadrature method. *Aerosp. Sci. Technol.* **2020**, *107*, 106261.
24. Shokrgozar, A.; Ghabussi, A.; Ebrahimi, F.; Habibi, M.; Safarpour, H. Viscoelastic dynamics and static responses of a graphene nanoplatelets-reinforced composite cylindrical microshell. *Mech. Based Des. Struct. Mach.* **2020**, *50*, 509–536. [CrossRef]
25. Liu, J.; Deng, X.; Wang, Q.; Zhong, R.; Xiong, R.; Zhao, J. A unified modeling method for dynamic analysis of GPL-reinforced FGP plate resting on Winkler-Pasternak foundation with elastic boundary conditions. *Compos. Struct.* **2020**, *244*, 112217.
26. Qian, W.-M.; Vahid, M.H.; Sun, Y.-L.; Heidari, A.; Barbaz-Isfahani, R.; Saber-Samandari, S.; Khandan, A.; Toghraie, D. Investigation on the effect of functionalization of single-walled carbon nanotubes on the mechanical properties of epoxy glass composites: Experimental and molecular dynamics simulation. *J. Mater. Res. Technol.* **2021**, *12*, 1931–1945.
27. Eyvazian, A.; Sebaey, T.A.; Żur, K.K.; Khan, A.; Zhang, H.; Wong, S.H. On the dynamics of FG-GPLRC sandwich cylinders based on an unconstrained higher-order theory. *Compos. Struct.* **2021**, *267*, 113879.
28. Zhao, S.; Zhang, Y.; Chen, D.; Yang, J.; Kitipornchai, S. Enhanced thermal buckling resistance of folded graphene reinforced nanocomposites with negative thermal expansion: From atomistic study to continuum mechanics modelling. *Compos. Struct.* **2022**, *279*, 114872.
29. Jiang, Y.; Li, L.; Hu, Y. A compatible multiscale model for nanocomposites incorporating interface effect. *Int. J. Eng. Sci.* **2022**, *174*, 103657.
30. Le, T.-T. Prediction of tensile strength of polymer carbon nanotube composites using practical machine learning method. *J. Compos. Mater.* **2021**, *55*, 787–811. [CrossRef]
31. Garg, A.; Belarbi, M.-O.; Tounsi, A.; Li, L.; Singh, A.; Mukhopadhyay, T. Predicting elemental stiffness matrix of FG nanoplates using Gaussian Process Regression based surrogate model in framework of layerwise model. *Eng. Anal. Bound. Elem.* **2022**, *143*, 779–795.
32. Rahman, A.; Deshpande, P.; Radue, M.S.; Odegard, G.M.; Gowtham, S.; Ghosh, S.; Spear, A.D. A machine learning framework for predicting the shear strength of carbon nanotube-polymer interfaces based on molecular dynamics simulation data. *Compos. Sci. Technol.* **2021**, *207*, 108627. [CrossRef]
33. Samui, P.; Roy, S.S.; Balas, V.E. *Handbook of Neural Computation*; Academic Press: Cambridge, MA, USA, 2017.
34. Ebrahimi, F.; Barati, M.R. Hygrothermal buckling analysis of magnetically actuated embedded higher order functionally graded nanoscale beams considering the neutral surface position. *J. Therm. Stress.* **2016**, *39*, 1210–1229. [CrossRef]
35. Ebrahimi, F.; Dabbagh, A. On thermo-mechanical vibration analysis of multi-scale hybrid composite beams. *J. Vib. Control* **2019**, *25*, 933–945.